# A novel semi-active actuator with tunable mass moment of inertia for <span style="color:green">noise control applications</span><span style="color:red">~~noise barriers or structural sound sources~~</span>

Stanislaw Wrona[a,*], Marek Pawelczyk[a], Li Cheng[b]

[a]*Silesian University of Technology, Department of Measurements and Control Systems, Gliwice, Poland*
[b]*Department of Mechanical Engineering, Hong Kong Polytechnic University, Hong Kong, China*

**Abstract**

Semi-active control approaches have been developed and employed for a variety of vibration-reduction applications, including adaptive vehicle suspensions, earthquake protection for civil structures, and more. These semi-active systems require significantly less energy than the corresponding active solutions, while continuing to provide a high level of performance, therefore they are an attractive approach. In the context of noise reduction barriers, semi-active control often refers to piezoelectric patches or stacks connected to shunt electric circuits in order to transform and dissipate mechanical energy. However, a different type of semi-active actuators can also be used to adapt the mechanical features of noise barriers in order to deal with varying noise properties. This paper proposes a novel semi-active actuator with tunable mass moment of inertia. When attached to a noise barrier, it can alter the resonant frequencies and mode shapes of the barrier in order to reduce acoustic radiation at dominant frequencies in the noise. As the presented results show, this actuator can enhance the transmission loss of a noise barrier for time-varying narrow-band noise by more than 10 dB in targeted frequency bands. Alternatively, the proposed actuator can be used to optimize acoustic radiation from a panel acting as a sound source. Both scenarios are considered and analyzed in this paper by employing mathematical modeling, experimental validation and numerical investigation.

*Keywords:* Semi-active control, mathematical modelling, acoustic radiation, vibrating plates, noise barriers

## 1. Introduction

Panels are often used in vibroacoustic applications as either noise barriers, which reduce the propagation of acoustic noise [1–5], or as structural sound sources [6, 7], which are highly resistant to unfavorable environmental conditions. In both use cases, <span style="color:red">~~since~~</span> the complex frequency response of most panels significantly impact their performance<span style="color:red">~~,~~</span><span style="color:red">.</span> <span style="color:green">Hence,</span> it would be beneficial to be able to shift and adapt the panel resonances in order to tune them to application requirements. For noise barriers, the effective transmission loss of <span style="color:green">a</span><span style="color:red">~~the~~</span> panel could be increased by altering mode shapes and tuning resonances, shifting them away from the dominant part of the noise spectrum. The authors have previously investigated such an approach and developed a passive

---

*Corresponding author
Email addresses:* `stanislaw.wrona@polsl.pl` (Stanislaw Wrona), `marek.pawelczyk@polsl.pl` (Marek Pawelczyk), `li.cheng@polyu.edu.hk` (Li Cheng)

**Nomenclature**

$a$ — length of the panel

$A(f, z_{a,1})$ — mean sound pressure amplitude

$b$ — width of the panel

$c$ — sound velocity in the air

$D$ — flexural rigidity of the panel

$E$ — Young's modulus of the panel

$f$ — frequency

$h$ — panel thickness

$I_{ax,i}, I_{ay,i}$ — moments of inertia of the $i$-th actuator

$k_e$ — acoustic wavenumber

$\mathbf{K}$ — stiffness matrix

$\mathbf{K}_b, \mathbf{K}_p$ — stiffness matrices corresponding to strain energy of the boundary restraints and the panel, respectively

$m_{a,i}$ — mass of the $i$-th actuator

$\mathbf{M}$ — mass matrix

$\mathbf{M}_a, \mathbf{M}_p$ — mass matrices corresponding to kinetic energy of actuators and the panel, respectively

$N$ — number of employed trial functions

$N_a$ — number of actuators bonded to the panel's surface, respectively

$p_{ext,i}(x, y, z)$ — modal sound pressure amplitude corresponding to $i$-th vibration mode

$P_{ext,i}$ — modal acoustic power corresponding to $i$-th vibration mode of the panel

$\mathbf{q}$ — generalized panel displacement vector

$S_e, S_p$ — surface enclosing the vibrating panel and surface of the panel, respectively

$t$ — time

$T, T_a, T_p$ — overall kinetic energy of the system and kinetic energies of actuators and the panel, respectively

$U, U_b, U_p$ — overall potential energy of the system and potential energies of the boundary restraints and the panel, respectively

$\mathbf{v}$ — modal displacement vector

$w(x, y, t)$ — displacement of the panel to the $z$-direction at time $t > 0$ and position $(x, y)$

$z_{a,i}$ — distance of the center of the mass of the $i$-th actuator from the panel mid-plane

$i, j, k$ — positive integers

$x, y, z$ — coordinates in the global Cartesian coordinate system

$x_{a,i}, y_{a,i}$ — coordinates of the $i$-th semi-active actuator

$\xi, \eta, \gamma$ — components of the acoustic wavevector

$\iota$ — imaginary number satisfying equation $\iota^2 = -1$

$\nu$ — Poisson's ratio of the panel

$\xi_{d,i}$ — damping coefficient corresponding to $i$-th mode of the panel

$\mathbf{\Xi}$ — damping matrix

$\rho_e, \rho$ — air density and mass density of the panel material, respectively

$\phi_i(x, y)$ — $i$-th time-invariant trial function

$\boldsymbol{\phi}$ — vector containing a set of time-invariant trial functions $\phi_i(x, y)$

$\mathbf{\Phi}$ — eigenvector matrix

$\mathbf{\Phi}_i$ — $i$-th eigenvector ($i$-th column in the eigenvector matrix $\mathbf{\Phi}$)

$\omega_i, \mathbf{\Omega}$ — $i$-th eigenfrequency and the eigenfrequencies matrix, respectively

solution by attaching additional passive masses and ribs to the surface of the barrier at locations determined by an optimization process [8–10]. On the other hand, in the case of a panel being utilized as a sound source, the radiated sound power could be significantly enhanced by favorable adaptation of resonances to the spectrum of the control signal [10]. Directivity pattern can also be included in the cost functions if required [11, 12]. It will be a subject of authors' future work.

In the case of vibrating panels, such adaptation has been performed using fixed passive elements, such as lumped masses or springs[12, 13]. However, it has rarely been approached in a semi-active manner, which allows a real-time tuning of panel response to the time-varying requirements. The authors believe that the ability to adapt to changing conditions would significantly enhance performance of the aforementioned noise barriers or sound sources. In the literature, Related semi-active approaches have been proposed for earthquake protection in civil structures [14, 15]. A sandwich plate with adjustable core layer thickness has also been proposed. This method employs a compressible open-cell foam core between panels and enables a compressible open-cell foam core between panels and enabling the adjustment of the structure's vibration behavior by changing the core compression using different actuation pressures [16].

This paper is intended to fill that gap and introduces a novel semi-active actuator with a tunable mass moment of inertia, capable of modulating the response of a panel during its operation. The actuator is based on an additional mass mounted on a guide (the body of the actuator), which is attached perpendicularly to the surface of the panel. The movable mass can be shifted closer to or further away from the panel surface, tuning its effective mass moment of inertia. The proposed semi-active device only requires energy for shifting the movable mass, otherwise the mass is self-blocked. The actuator can shift the resonant frequencies and alter the mode shapes of the entire panel. These shapes determine the acoustic radiation efficiency of particular modes [10].

The proposed actuator enables an adaptation of the frequency-dependent transmission loss of a barrier to the current noise spectrum. The noise spectrum can be easily monitored, allowing, e.g., a minimization of the sound radiation of the barrier in the targeted frequency bands. Such an approach is intended to the efficient reduction of transmission of non-stationary narrow-band noise, which is commonly encountered in real-life, both in the case of industrial devices and household appliances. The proposed solution can greatly enhance the effective transmission loss of a barrier, while being significantly lighter and requiring less space than vibration absorbers or Helmholtz resonators (which can be bulky when tuned for low frequencies). Simultaneously, it is less demanding in terms of system complexity and in energy required compared to a fully active approach.

The proposed actuator can also be used to optimize acoustic radiation from a panel acting as a sound source. In this research, in addition to the way in which the panel would be excited, the optimization of acoustic radiation efficiency for particular tonal frequencies is considered. Such semi-active tuning of a sound source has many potential applications due to the reduction of energy consumption; for example it could be used in support of an active noise reduction system by tuning the acoustic radiation of secondary sources, forming a hybrid active/semi-active system. The complete design of such a hybrid system is beyond the scope of this paper.

When employing the proposed actuator, it is important to consider its placement on the panel surface. In this paper, four cost functions are proposed and evaluated for optimization of the location of the actuators—two cost functions are dedicated to the case of a noise barrier, and two are intended for a sound source. Depending on the objective of the considered application, different placements and configurations of the actuator allow for optimal performance. For this purpose, the concept of an equally weighted modal response is introduced into the optimization process in order to provide more general solutions.

This paper is organized as follows. Section 2 introduces a mathematical model of the panel and the proposed semi-active actuators, including the impact of mass loading. Section 3 discusses the results of an experimental validation of the model. Section 4 presents numerical simulation studies based on the validated model, providing analysis and insight into various practical aspects including optimization of the location of the actuator according to the proposed cost functions and the resulting acoustic performance. Section 5 presents laboratory experiments performed for the optimal configuration followed from the simulation studies. Section 6 summarizes the obtained results and conclusions.

## 2. Modeling of the vibroacoustic system

A model of the vibroacoustic system with semi-active actuators is detailed in this section. Figure 1 gives a schematic representation of the system. The derivation is based on a description of the free vibrations of an isotropic, rectangular plate with additional masses bonded to its
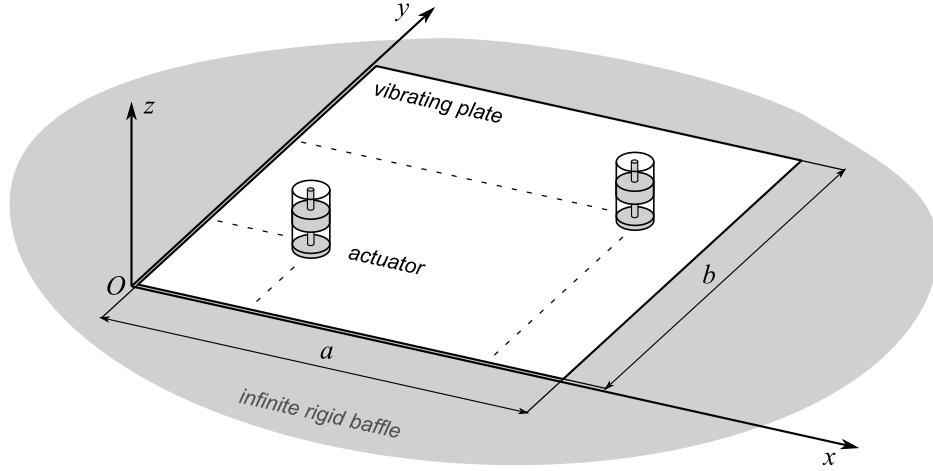
Figure 1: A schematic representation of the vibrating plate with semi-active actuators, placed in an infinite rigid baffle.

surface. The Kirchhoff-Love theory of thin plates is used for this purpose [17]. The Rayleigh-Ritz method is used to define an approximate solution to the eigenvalue equation, giving the natural frequencies and mode shapes of the vibrating system [18]. Finally, an appropriate Green's function is used to estimate the acoustic radiation from the obtained modes.

*Modeling of the panel vibration*

For an isotropic and homogeneous panel in the $x$–$y$ plane, in a reference stress-free state, free vibrations are governed by the differential equation [17]

$$D\nabla^4 w + \rho h \ddot{w} = 0 \,, \tag{1}$$

where

$$x \in (0, a) \,, \quad y \in (0, b) \,. \tag{2}$$

In Eqs. (1)-(2), the function $w(x, y, t)$ denotes the displacement of the panel from the reference state in the $z$-direction at time $t > 0$ and position $(x, y)$; the lengths of the rectangular panel edges are assumed to be equal to $a$ and $b$, respectively; $D = Eh^3/[12(1 - v^2)]$ is the flexural rigidity; $E$ is the Young's modulus; $v$ is the Poisson ratio; $\rho$ is the mass density of the panel material; and $h$ is the panel thickness.

Considering only the transverse motion and neglecting the effect of rotary inertia, the kinetic and strain energies of the panel, $T_p$ and $U_p$, can be written as

$$T_p = \frac{\rho h}{2} \iint\limits_{S_p} \dot{w}^2 \mathrm{d}x \, \mathrm{d}y \,, \tag{3a}$$

$$U_p = \frac{D}{2} \iint\limits_{S_p} \left\{ \left( \frac{\partial^2 w}{\partial x^2} \right)^2 + \left( \frac{\partial^2 w}{\partial y^2} \right)^2 + 2v \frac{\partial^2 w}{\partial x^2} \frac{\partial^2 w}{\partial y^2} + 2(1 - v) \left( \frac{\partial^2 w}{\partial x \partial y} \right)^2 \right\} \mathrm{d}x \, \mathrm{d}y \,, \tag{3b}$$

where the integration region $S_p$ is over the surface of the panel.

To reflect the fact that the mounting of the panels is often imperfect (neither simply-supported nor fully-clamped), boundary conditions which are elastically restrained against rotation are

4

adopted. They are represented by rotational springs distributed uniformly along panel edges and possessing a uniform spring constant $k_b$. The classical boundary conditions of the panel can be obtained as limiting cases when the spring constant $k_b$ approaches its natural limits of zero or infinity, leading to simply-supported or fully-clamped boundary conditions, respectively. The strain energy stored in the rotational springs, $U_b$, is given by:

$$U_b = \frac{k_b}{2} \left[ \int_0^b \left\{ \left(\frac{\partial w}{\partial x}\right)^2 \bigg|_{x=0} + \left(\frac{\partial w}{\partial x}\right)^2 \bigg|_{x=a} \right\} \mathrm{d}y + \int_0^a \left\{ \left(\frac{\partial w}{\partial y}\right)^2 \bigg|_{y=0} + \left(\frac{\partial w}{\partial y}\right)^2 \bigg|_{y=b} \right\} \mathrm{d}x \right]. \tag{4}$$

The Rayleigh-Ritz method, which is used in this work to find an approximate solution of the differential system, is based on the definition of an energy functional. Therefore the definitions of the kinetic and strain energies of the panel are of particular importance.

*Semi-active actuators*

The panel considered in this paper is the subject of semi-active control by way of semi-active actuators attached to its surface. The role of the actuators is to influence the dynamic response of the panel, thus they have to be included in the mathematical modeling. For the sake of brevity, the mathematical model of the actuators is presented independently of the model of the vibrating panel. In particular, only the kinetic and potential energies related to the actuators are defined, as these are necessary for the Rayleigh-Ritz method [18].

Because the dimensions of the considered actuators are assumed to be significantly smaller than the dimensions of the panel, they can be modeled as point masses located at a specified distance from the panel surface, while maintaining satisfactory accuracy for the purpose of frequency response shaping [8, 19]. This approach includes the mass moment of inertia of the actuator and related bending moments acting on the panel. The body of the actuators is assumed to be perfectly rigid. In the case of larger elements or elements of an alternative structure, a more complex representation in the mathematical model would be required in order to accurately reflect the physical response. The effect of strain caused by the bonding of semi-active actuators to the panel surface is also neglected in the current study. This does not inherently limit the proposed optimization method, because the model could be extended to include this effect if necessary. Furthermore, perfect bonding is assumed, such that the total energy introduced to the system by the actuators is taken to be their kinetic energy expressed as

$$T_a = \sum_{i=1}^{N_a} \left\{ \frac{m_{a,i}}{2} \dot{w}^2 + \frac{I_{ax,i}}{2} \frac{\partial \dot{w}^2}{\partial x} + \frac{I_{ay,i}}{2} \frac{\partial \dot{w}^2}{\partial y} \right\} \Bigg|_{\substack{x=x_{a,i} \\ y=y_{a,i}}}, \tag{5}$$

where $N_a$, $m_{a,i}$, $I_{ax,i}$, $I_{ay,i}$, $x_{a,i}$ and $y_{a,i}$ are, respectively, the number of actuators bonded to the panel surface, the mass of the $i$-th actuator, the moments of inertia of the $i$-th actuator, and the coordinates of the $i$-th actuator. Considering the actuators as point masses, the moments of inertia are $I_{ax,i} = I_{ay,i} = m_{a,i} z_{a,i}^2$, where $z_{a,i}$ is the distance of the center of the mass of the $i$-th actuator from the panel mid-plane, resulting in the following expression for the kinetic energy $T_a$

$$T_a = \sum_{i=1}^{N_a} \left[ \frac{m_{a,i}}{2} \left\{ \dot{w}^2 + z_{a,i}^2 \left( \frac{\partial \dot{w}^2}{\partial x} + \frac{\partial \dot{w}^2}{\partial y} \right) \right\} \right] \Bigg|_{\substack{x=x_{a,i} \\ y=y_{a,i}}}, \tag{6}$$

*The Rayleigh-Ritz method*

The Rayleigh-Ritz method is used in this paper to calculate an approximate solution of the presented differential system, obtaining its natural frequencies and mode shapes. To use this method the total energy of the system and carefully-selected trial functions need to be defined. The energy functionals have already been derived in the preceding text. The characteristic orthogonal polynomials, with the properties of Euler-Bernoulli beam functions, are used as the trial functions. The procedure for forming orthogonal polynomial trial functions for rectangular plates is described in detail in [20]. More detailed information regarding the Rayleigh-Ritz method itself is provided in [18].

For free vibration of the panel, the solution of $w$ can be expressed in the required form using a sum over a predetermined set of admissible trial functions

$$w(x, y, t) = \sum_{i=1}^{N} \phi_i(x, y) q_i(t) = \boldsymbol{\phi}^{\mathrm{T}} \mathbf{q} \,, \tag{7}$$

where $\mathbf{q}$ is a generalized panel displacement vector; $\boldsymbol{\phi}$ is a vector which represents a set of time-invariant trial functions $\phi_i(x, y)$; and the superscript T denotes the transpose. All of these vectors have dimensions $(N \times 1)$, where $N$ is the number of trial functions used.

*Total energy definition*

Utilizing Eq. (7), the total kinetic and potential energies $T$ and $U$ following from Eqs. (3) and (6) can be written as functions of the generalized panel displacement vector $\mathbf{q}$, the mass matrix $\mathbf{M}$ of dimensions $(N \times N)$ and the stiffness matrix $\mathbf{K}$ of dimensions $(N \times N)$ as

$$T = T_p + T_a = \frac{1}{2} \dot{\mathbf{q}}^{\mathrm{T}} \mathbf{M} \dot{\mathbf{q}} \,, \qquad U = U_p + U_b = \frac{1}{2} \mathbf{q}^{\mathrm{T}} \mathbf{K} \mathbf{q} \,. \tag{8}$$

The overall mass matrix $\mathbf{M}$ is calculated as the sum of the matrices related to the different energy components

$$\mathbf{M} = \mathbf{M}_p + \mathbf{M}_a \,, \tag{9}$$

where $\mathbf{M}_p$ and $\mathbf{M}_a$ are related to the panel and the semi-active actuators, respectively. The elements of the mass matrices introduced in Eq. (9) are defined as

$$M_{p,ij} = \rho h \iint_{S_p} \phi_i \phi_j \mathrm{d}x \, \mathrm{d}y \,, \tag{10a}$$

$$M_{a,ij} = \sum_{k=1}^{N_a} \left[ m_{a,k} \left\{ \phi_i \phi_j + z_{a,i}^2 \left( \frac{\partial \phi_i}{\partial x} \frac{\partial \phi_j}{\partial x} + \frac{\partial \phi_i}{\partial y} \frac{\partial \phi_j}{\partial y} \right) \right\} \right] \Bigg|_{\substack{x=x_{a,k} \\ y=y_{a,k}}} \,. \tag{10b}$$

The overall stiffness matrix $\mathbf{K}$ is also calculated as the sum of matrices relating to the different components

$$\mathbf{K} = \mathbf{K}_p + \mathbf{K}_b \,, \tag{11}$$

where $\mathbf{K}_p$ and $\mathbf{K}_b$ belong to the panel and boundary restraints, respectively. The elements of the stiffness matrices introduced in Eq. (11) are defined as

$$K_{p,ij} = D \iint\limits_{S_p} \left\{ \frac{\partial^2 \phi_i}{\partial x^2} \frac{\partial^2 \phi_j}{\partial x^2} + \frac{\partial^2 \phi_i}{\partial y^2} \frac{\partial^2 \phi_j}{\partial y^2} + 2\nu \frac{\partial^2 \phi_i}{\partial x^2} \frac{\partial^2 \phi_j}{\partial y^2} + 2(1-\nu) \frac{\partial^2 \phi_i}{\partial x \partial y} \frac{\partial^2 \phi_j}{\partial x \partial y} \right\} \mathrm{d}x\,\mathrm{d}y \,, \qquad (12a)$$

$$K_{b,ij} = k_b \left[ \int_0^b \left\{ \left( \frac{\partial \phi_i}{\partial x} \frac{\partial \phi_j}{\partial x} \right)\Big|_{x=0} + \left( \frac{\partial \phi_i}{\partial x} \frac{\partial \phi_j}{\partial x} \right)\Big|_{x=a} \right\} \mathrm{d}y + \int_0^a \left\{ \left( \frac{\partial \phi_i}{\partial y} \frac{\partial \phi_j}{\partial y} \right)\Big|_{y=0} + \left( \frac{\partial \phi_i}{\partial y} \frac{\partial \phi_j}{\partial y} \right)\Big|_{y=b} \right\} \mathrm{d}x \right].$$
$$(12b)$$

*Equation of the vibrating structure and its harmonic solution*

Having defined the stiffness and mass matrices, by using the Lagrange equation of the second kind the equation of a vibrating structure can be obtained as

$$\mathbf{M}\ddot{\mathbf{q}} + \mathbf{K}\mathbf{q} = \mathbf{0}_N \,, \qquad (13)$$

where $\mathbf{0}_N$ is a zero vector, with dimensions $(N \times 1)$. The harmonic solution to Eq. (13) gives the eigenvector matrix $\mathbf{\Phi}$ with dimensions $(N \times N)$ and $N$ eigenfrequencies $\omega_i$. Replacing $\mathbf{q}^{\mathrm{T}}$ by $\mathbf{\Phi}\mathbf{v}$, and multiplying Eq. (13) on the left by $\mathbf{\Phi}^{\mathrm{T}}$ gives

$$\mathbf{\Phi}^{\mathrm{T}}\mathbf{M}\mathbf{\Phi}\ddot{\mathbf{v}} + \mathbf{\Phi}^{\mathrm{T}}\mathbf{K}\mathbf{\Phi}\mathbf{v} = \mathbf{0}_N \,, \qquad (14)$$

where $\mathbf{v}$ denotes the modal displacement vector of dimensions $(N \times 1)$:

$$\mathbf{v} = [v_1, v_2, \dots, v_N]^{\mathrm{T}} \,. \qquad (15)$$

Taking advantage of the orthonormality of the eigenvectors in matrix $\mathbf{\Phi}$, the modal mass matrix becomes a unit matrix $\mathbf{I}_N$ of dimensions $(N \times N)$ and the corresponding modal stiffness matrix becomes a diagonal matrix $\mathbf{\Omega}$ of $N$ eigenvalues $\omega_i^2$ [21], which gives

$$\mathbf{\Phi}^{\mathrm{T}}\mathbf{M}\mathbf{\Phi} = \mathbf{I}_N \,, \qquad (16a)$$

$$\mathbf{\Phi}^{\mathrm{T}}\mathbf{K}\mathbf{\Phi} = \mathbf{\Omega} = \left[ \mathrm{diag}(\omega_1^2, \omega_2^2, \dots, \omega_N^2) \right] \,. \qquad (16b)$$

Then, substituting Eq. (16) in Eq. (14) gives

$$\ddot{\mathbf{v}} + \mathbf{\Omega}\mathbf{v} = \mathbf{0}_N \,. \qquad (17)$$

To provide a better representation of the behavior of a real system, this is extended to

$$\ddot{\mathbf{v}} + \mathbf{\Xi}\dot{\mathbf{v}} + \mathbf{\Omega}\mathbf{v} = \mathbf{0}_N \,, \qquad (18)$$

where $\mathbf{\Xi}\dot{\mathbf{v}}$ is a term introduced to include the damping in the system, and $\mathbf{\Xi}$ is a diagonal matrix of dimensions $(N \times N)$ defined as

$$\mathbf{\Xi} = \left[ \mathrm{diag}(2\xi_{d,1}\omega_1, 2\xi_{d,2}\omega_2, \dots, 2\xi_{d,N}\omega_N) \right] \,. \qquad (19)$$

In Eq. (19), the damping ratios, $0 < \xi_{d,i} < 1$, are calculated using the thermoelastic damping model for elastic plates described in [22]. The effects of damping could also be included at the beginning of the derivation in the form of complex bending rigidities. However, this would significantly complicate the derivation. Introducing it instead at this stage preserves the brevity of the derivation and leads to an equivalent solution [23].

7

*Acoustic radiation*

An estimate of the radiated acoustic power corresponding to the $i$-th vibration mode of the panel under consideration is derived in this subsection. In the scenario considered, it is assumed that the panel is placed in an infinite rigid baffle, as shown in Fig. 1. Adopting an appropriate Green's function (derived in [24]) the modal sound pressure amplitude $p_{ext,i}(x, y, z)$ can be calculated for $z > 0$ as

$$p_{ext,i}(x, y, z) = \frac{k_e a\, b}{4\pi^2} \rho_e c \iint\limits_{-\infty}^{+\infty} \exp\left[\iota\left(\xi x + \eta y + \gamma z\right)\right] M_i(\xi, \eta) \frac{\mathrm{d}\xi\, \mathrm{d}\eta}{\gamma} , \qquad (20)$$

where

$$M_i(\xi, \eta) = \frac{-2\iota\,\omega_{c,i}}{ab} \iint\limits_{S_p} \psi_{b',i} \exp\left[-\iota\left(\xi x + \eta y\right)\right] \mathrm{d}x\, \mathrm{d}y . \qquad (21)$$

In Eqs. (20)-(21) the symbol $k_e = \omega_{c,i}/c$ is the acoustic wavenumber; $\xi$, $\eta$ and $\gamma$ are the components of the acoustic wavevector; $\rho_e$ and $c$ are the density of air and the sound speed in air, respectively; $\iota$ is the imaginary number $\sqrt{-1}$; $\mathbf{\Phi}_i$ is the $i$-th eigenvector (the $i$-th column in the eigenvector matrix $\mathbf{\Phi}$).

To determine an estimate of the modal acoustic power, $P_{ext,i}$, the squared modal sound pressure under free-field and far-field conditions, $p_{ext,i}(x, y, z)$, can be averaged over a surface $S_{ext}$, which encloses the vibrating panel [10]. Hence, the modal acoustic power $P_{ext,i}$ can be expressed as

$$P_{ext,i} = \iint\limits_{S_{ext}} \frac{\left|p_{RMS,i}(x, y, z)\right|^2}{\rho_e c} \mathrm{d}S_{ext} , \qquad (22)$$

where $p_{RMS,i}(x, y, z) = \frac{1}{\sqrt{2}} p_{ext,i}(x, y, z)$ is the root mean square of $p_{ext,i}(x, y, z)$.

## 3. Experimental validation

This section presents the results of an experimental validation of the model developed in the previous section. A rectangular steel plate with a prototype of the proposed semi-active actuator was used for this purpose. The plate was mounted to a heavy concrete box and excited with a loudspeaker placed inside the box. The loudspeaker was driven to generate a broadband, random noise (a band-limited white noise). The concrete walls of the box provided high noise attenuation, and hence most of the acoustic energy which was transmitted outside the box was transmitted through the steel plate. The acoustic modes of the cavity inside the box affected to some extent the acoustic excitation distribution over the panel, however, all of the vibration modes of the panel, theoretically expected in the considered frequency range, were excited enough to be captured with the laboratory equipment. A photograph of the laboratory setup is shown in Fig. 2a. The dimensions of the panel area that was free to vibrate (i.e. the area inside the clamping frame) were 0.420 m × 0.390 m.

The schematic representation of the actuator prototype is presented in Fig. 2b. The body of the actuator was made from a poly-methyl methacrylate (PMMA) tube, guiding the well-fitted movable mass inside it. The mass, with a threaded hole inside, is shifted using a threaded rod, thus adjusting the distance between the mass and the panel $z_{a,1}$. The threaded rod is rotated through a micro motor and a belt transmission. The threaded rod is mounted in a ball bearing at

the base of the actuator. The actuator is attached to the panel surface using a neodymium magnet, also attached to the base of the actuator. The micro motor is equipped with an encoder allowing a precise determination of the movable mass current position. Although the mechanical design of this prototype could still be improved, it is a clear practical realization of the proposed type of semi-active actuator. The distance $z_{a,1}$ should be automatically adjusted by a dedicated controller, calculating the optimal distance $z_{a,1}$ based on continuously monitored frequency spectrum of the noise.

The proposed actuator can alter natural frequencies and mode shapes of the panel by adjusting the distance $z_{a,1}$. The underlying mechanisms behind this phenomena are based on increasing the modal mass of the modes with the increased mass moment of inertia of the actuator. However, in order for the mass moment of inertia of the actuator to affect the particular mode, the actuator should "swing" while the mode vibrates. It is determined by the location of the actuator in relation to the particular mode shape – the rotations of the panel surface are highest at the nodal lines, while they are absent at the anti-nodes (at the anti-nodes the motion of the panel surface is solely translational). The increase of the modal mass due to actuator is local (not uniform), hence apart from shifting the natural frequency of the mode, the mode shape is also altered in an irregular manner, what also effects the modal acoustic radiation efficiency.

The panel and the semi-active actuator at the moment of the experiment can be described by the following parameters (cf. Section 2 for the meaning of the symbols)

$$
\begin{aligned}
a &= 0.420 \text{ m}, & b &= 0.390 \text{ m}, & h &= 0.001 \text{ m}, \\
E &= 210 \text{ GPa}, & \rho_p &= 7850 \text{ }^{\text{kg}}/_{\text{m}^3}, & \nu &= 0.3, \\
k_b &= 340 \text{ N/rad}, \\
c_p &= 343 \text{ }^{\text{m}}/_{\text{s}}, & \rho_p &= 1.21 \text{ }^{\text{kg}}/_{\text{m}^3}, \\
m_{a,1} &= 0.055 \text{ m}, & x_{a,1} &= 0.100 \text{ m}, & y_{a,1} &= 0.100 \text{ m}, \\
z_{a,1} &= 0.012 \text{ m}.
\end{aligned}
$$
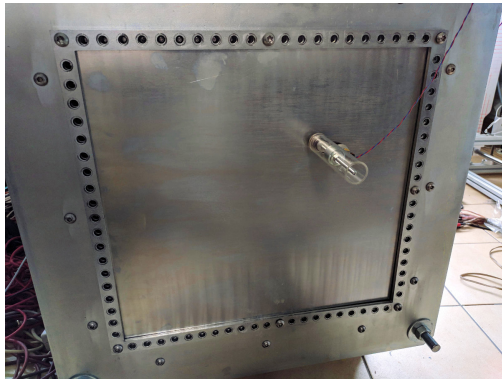


(a) A photograph of the heavy concrete box with a panel and a mounted semi-active actuator.
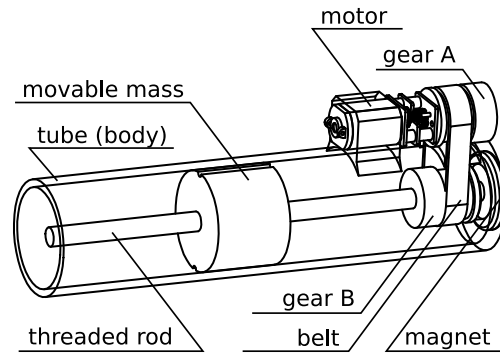
(b) A schematic of the semi-active actuator (own design).

Figure 2: A photograph and a schematic of the laboratory setup.

The value of $k_b$ was identified based on preliminary experiments according to procedure described in [25], which generally relies on employment of optimization algorithm minimizing discrepancies between mathematical model and experimental results in terms of natural frequencies and mode shapes.

For the purpose of model validation, the structural response of vibrating panel was experimentally measured using a Polytec PDV-100 laser vibrometer mounted on an automatic positioning system developed by the authors. The positioning system allowed precise movement of the carriage with the vibrometer along both horizontal and vertical axes. The results obtained are compared with theoretical predictions in the following Subsection 3.1.

Moreover, the modeling of the acoustic radiation from the panel was also validated. For this purpose, two Beyerdynamic MM1 measurement microphones were mounted on the carriage along with the laser vibrometer. Although this validation was successfully completed during this research, for the sake of conciseness the verification data has been omitted from the current paper because the acoustic radiation model has already been verified in [10] for a related scenario, and the analogous verification data was published there.

### 3.1. Vibrations of the panel with semi-active actuator

Vibration measurements of the panel were taken over a uniform grid of $22 \times 20$ points, giving a total of 440 points, spaced at intervals of 0.02 m, which is sufficiently dense for the considered frequency range. The measurement grid covered the whole surface of the panel. After completing the measurements, the frequency analysis for all points was performed, and the estimated signal energy obtained for particular frequencies of structural resonances (frequencies of consecutive modes) at all measurement locations was aggregated in order to extract the mode shapes.

A comparison between the results measured experimentally and those calculated using the mathematical model is presented in Fig. 3. From these results it can be seen that the calculations and measurements are coherent, in terms of both the natural frequencies and mode shapes, and the model can therefore be used for the optimization problem and simulation studies presented in the following section.

## 4. Simulation studies

Simulations have been performed by adopting the panel parameters described in Section 3. Frequencies up to 300 Hz are considered, thus approximately the first ten eigenmodes of the panel are included in the considered scope. For the unloaded panel, ~~the~~ frequency responses obtained from the model are shown in Fig. 4. The acoustic response shown (denoted hereafter as $A(\cdot)$) is the mean sound pressure amplitude obtained by averaging over a uniform measurement grid of $26 \times 20$ points, giving a total of 520 points, spaced at intervals of 0.04 m. The measurement grid was 1.00 m wide and 0.76 m high, and 0.1 m from the panel surface. This choice of measurement grid follows from the experimental setup used for modeling validation, and is described in more detail in [10]. Such averaging provides a reliable estimate of the overall acoustic radiation generated by the panel. The structural (vibration) response shown is the mean vibration velocity obtained by averaging over a measurement grid of $22 \times 20$ points, giving a total of 440 points, spaced at intervals of 0.02 m, hence covering the whole surface of panel.

In all presented simulations, the excitation of the panel was obtained by directly applying an equal excitation to all loaded structural modes, instead of explicitly simulating a specific acoustic or structural excitation. Thus, the obtained responses have been named *equally weighted modal*
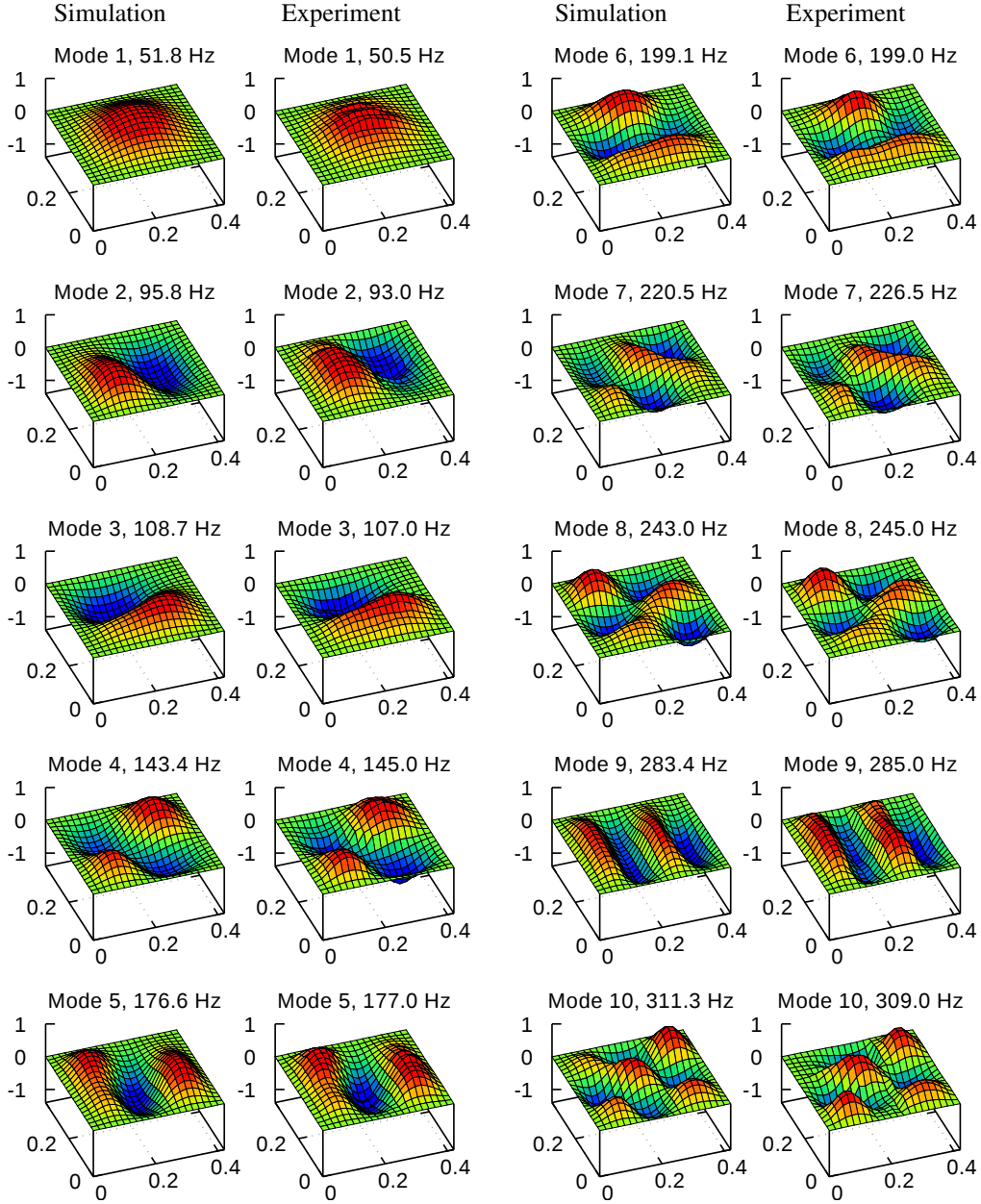
Figure 3: A comparison of the first 10 natural frequencies, and mode shapes calculated with the mathematical model and experimentally measured operational vibration shapes of the loaded panel. The panel was a 1 mm thick steel plate with an additional mass $m_{a,1} = 0.055$ kg attached at $x_{a,1} = 0.10$ m, $y_{a,1} = 0.10$ m, with a center of mass in a distance $z_{a,1} = 0.012$ m from the panel mid-plane. Size of the panel is in [m], and the z-axis depicts normalized amplitude.

11

*responses*, in order to better distinguish them from usual system responses. Such approach is motivated by the objective to design a barrier (or a sound source) dedicated for any kind of excitation (within the assumed frequency band), which is unknown and theoretically can excite any of the modes. Therefore, within the process of optimization of actuator's location, all of the modes should be well reflected in the simulated scenario in order to ensure that the actuator is able to sufficiently influence each mode of the panel. Moreover, it has been assessed that it is the best scenario to "prepare" the barrier and evaluate its performance for any kind of excitation, providing a more general solution as the result of the optimization process.

The movable mass is a replaceable component of the actuator and it can be changed during the preparation phase to achieve a desired mass. In the optimization process, the total mass of the semi-active actuator (including the body of the device) is limited to a maximum value of 0.2 kg (15% of the panel weight, which is equal to 1.3 kg). The real actuator used in the experimental setup may have some imperfections compared to simulations, e.g., the total mass may slightly differ, the distance of the center of the mass of the actuator from the panel mid-plane $z_{a,1}$ may differ to some extent, also the mounting may be not perfectly rigid, etc. However, the achieved consistency between the simulations and experiments is high (cf. Fig. 3), hence, the authors are confident that any potential inaccuracies should be small enough to not affect the overall performance of the proposed solution. Nevertheless, for the semi-active control purpose, experimental frequency responses should be used instead of theoretically predicted ones to take into account any potential inaccuracies.

Having in mind potential practical applications, the control system should employ as few actuators as possible to achieve the imposed objective. The simpler solution is often more attractive. Hence, in the simulation studies, optimization is performed for a single actuator, which proved to be sufficient for the considered objectives. Nevertheless, more actuators can be considered as well to enhance the performance further.

The distance ~~of the center of the mass of the actuator from the panel mid-plane~~ $z_{a,1}$ is assumed to be adjustable in a range between 0.01 m and 0.10 m (in practice these limits will depend on the chosen configuration of the actuator and the setup as a whole). For the purpose of optimization, the continuous domain of $z_{a,1}$ was discretized with a step size of 0.01 m, thus considering 10
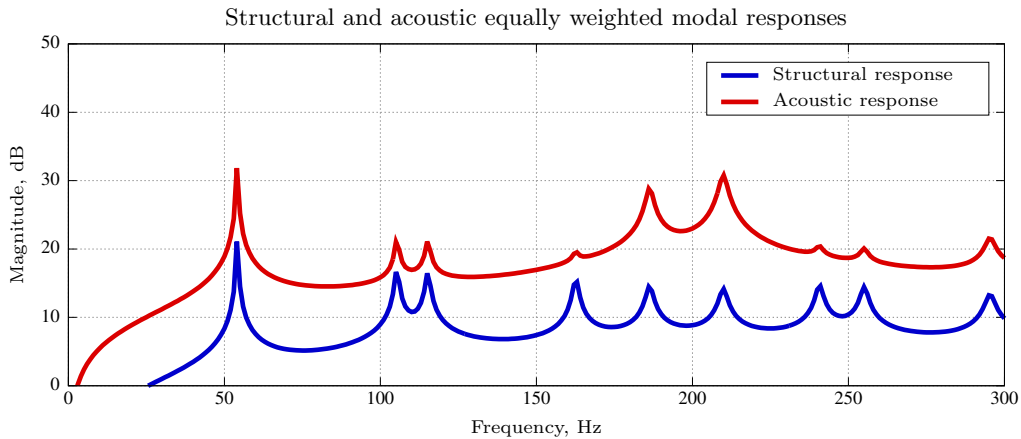


Figure 4: Structural (vibration) and acoustic equally weighted modal responses of the unloaded panel (without the semi-active actuator).

Table 1: Comparison of modal acoustic power $P_{ext,i}$ in [dB] of first ten eigenmodes of the panel in relation to the distance $z_{a,1}$.

| $z_{a,1}$ | Mode number | | | | | | | | | |
|---|---|---|---|---|---|---|---|---|---|---|
| | 1 | 2 | 3 | 4 | 5 | 6 | 7 | 8 | 9 | 10 |
| 0.01 | 20.4 | 15.1 | 13.8 | 11.3 | 24.8 | 21.2 | 20.8 | 18.6 | 19.9 | 9.9 |
| 0.02 | 20.4 | 15.2 | 13.8 | 11.1 | 24.4 | 22.1 | 22.3 | 19.9 | 20.5 | 16.5 |
| 0.03 | 20.4 | 15.3 | 13.8 | 11.0 | 22.9 | 24.1 | 22.6 | 20.5 | 21.7 | 16.5 |
| 0.04 | 20.3 | 15.5 | 13.9 | 12.6 | 18.2 | 25.2 | 24.6 | 21.5 | 22.0 | 15.8 |
| 0.05 | 20.2 | 15.8 | 14.0 | 17.2 | 13.9 | 22.0 | 25.4 | 19.1 | 22.0 | 15.1 |
| 0.06 | 20.1 | 16.2 | 14.5 | 19.4 | 18.8 | 18.2 | 25.5 | 18.7 | 22.0 | 14.6 |
| 0.07 | 20.0 | 16.6 | 17.1 | 21.2 | 15.4 | 16.5 | 25.6 | 18.6 | 22.1 | 14.4 |
| 0.08 | 19.8 | 16.3 | 20.4 | 20.2 | 14.2 | 15.7 | 25.6 | 18.6 | 22.1 | 14.3 |
| 0.09 | 19.6 | 15.1 | 22.3 | 16.5 | 14.0 | 15.3 | 25.6 | 18.6 | 22.1 | 14.2 |
| 0.10 | 19.3 | 13.6 | 23.2 | 13.9 | 14.0 | 15.0 | 25.6 | 18.6 | 22.1 | 14.1 |

possible settings of $z_{a,1}$ for the semi-active actuator. The aim of the optimization is to find the optimal location for the actuator on the panel surface, considering all available settings of $z_{a,1}$. It is also assumed for optimization purposes that only a tonal noise will be attenuated by the barrier, or that only a tonal sound should be emitted by the panel. Thus, during the cost function evaluation, each frequency in the considered range is evaluated individually (incremented by steps of 1 Hz and ranging up to 300 Hz) in choosing the most suitable setting of $z_{a,1}$.

A population-based memetic algorithm was used to carry out the optimization. For each optimization process, the population consisted of 300 individuals (considered solutions), the maximum number of generations was set to 15, and the probabilities of crossover, mutation and individual learning were 0.20, 0.30 and 0.06, respectively. For a detailed introduction to memetic algorithms, please refer to [26].

### 4.1. Semi-active noise barrier

The first scenario considered is the panel used as a semi-active noise barrier, which when excited should radiate noise to the environment on its other side as little as possible (considering excitation originating from both air-borne sound and structural vibrations). To this end, the acoustic radiation of the panel should be minimized over a wide frequency range. This objective is encapsulated in the following cost function

$$J_1 = \sum_{f=1}^{f=f_{max}} \left[ \min_{z_{a,1}} A(f, z_{a,1}) \right] , \qquad (23)$$

where $f_{max}$ is a maximum frequency limiting the frequency range of interest; and $A(f, z_{a,1})$ is the mean sound pressure amplitude as a function of both frequency and the parameter $z_{a,1}$. The cost function $J_1$ takes into account the overall acoustic radiation of the panel. To evaluate the cost function, the maximum frequency was set to $f_{max} = 300$ Hz.

The memetic algorithm achieved a solution with the actuator placed at $x_{a,1} = 0.287$ m, $y_{a,1} = 0.098$ m, with mass $m_{a,1} = 0.081$ kg. The results of this optimization are shown in Figs. 5-6. To analyze the obtained configuration, it is instructive to first consider Fig. 5, which presents all ten structural and acoustic responses obtained for different values of $z_{a,1}$. The fundamental
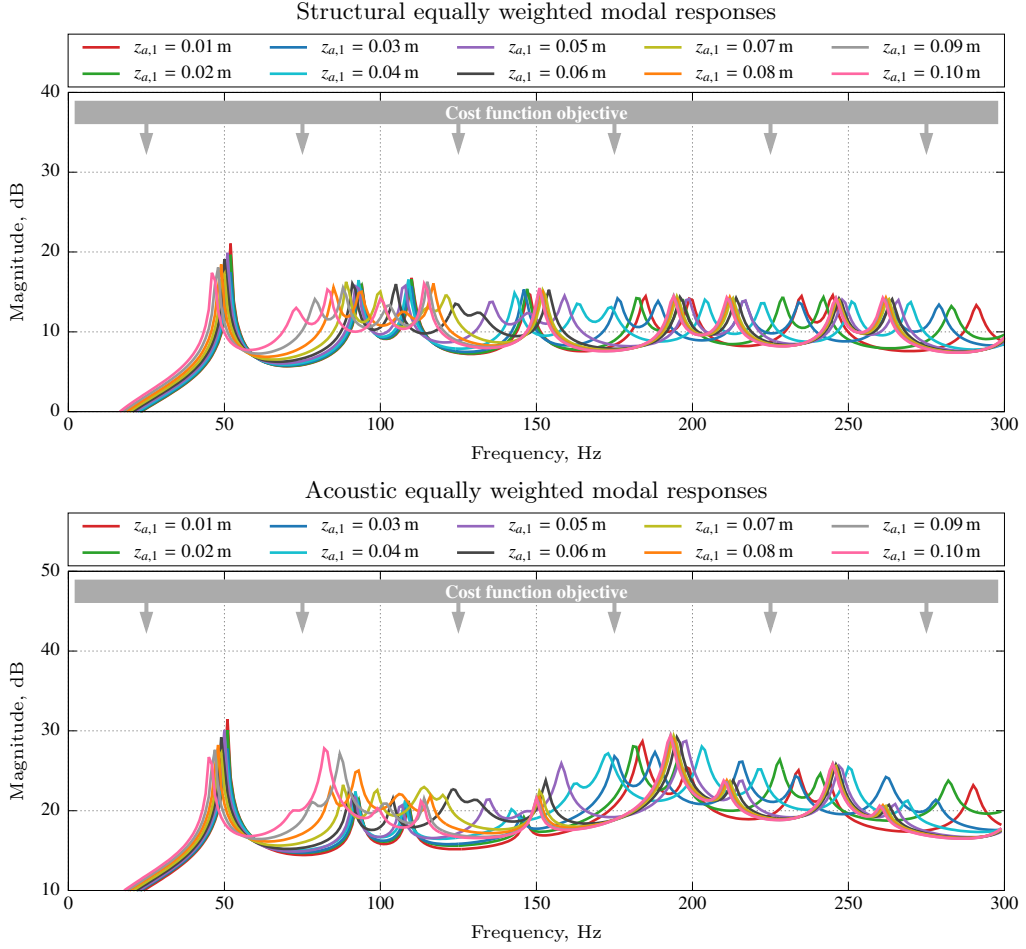
Figure 5: Individual structural (vibration) and acoustic equally weighted modal responses of the panel, obtained for optimization index $J_1$, with the actuator set for different $z_{a,1}$, in the range from 0.01 m to 0.10 m, incremented by 0.01 m. The actuator was attached at $x_{a,1} = 0.287$ m, $y_{a,1} = 0.098$ m, with $m_{a,1} = 0.081$ kg.

frequency gradually decreases when $z_{a,1}$ increases. For the following modes it is less clear due to mode superposition and changes in the order of peaks, however, similar phenomena occur. In addition to shifting the natural frequencies, changing $z_{a,1}$ can also strongly affect the amplitude of individual modes in the acoustic response due to the alteration of the modal acoustic radiation efficiency. The modal acoustic power $P_{ext,i}$ of first ten eigenmodes of the panel in relation to the distance $z_{a,1}$ has been compared in Tab. 1. Also note that a shift in the distance $z_{a,1}$ has a stronger effect on modes, which have nodal lines of their mode shapes near the actuator (the rotation amplitude of the panel surface is highest at the nodal lines).

Having all of the acoustic responses stored, an optimal value of $z_{a,1}$ can be determined for each frequency. The optimal solution (obtained by taking a minimum value of all responses for each frequency) is presented in Fig. 6 with a black solid line. The individual responses for different $z_{a,1}$ are presented with a light gray color for reference, while the acoustic response of
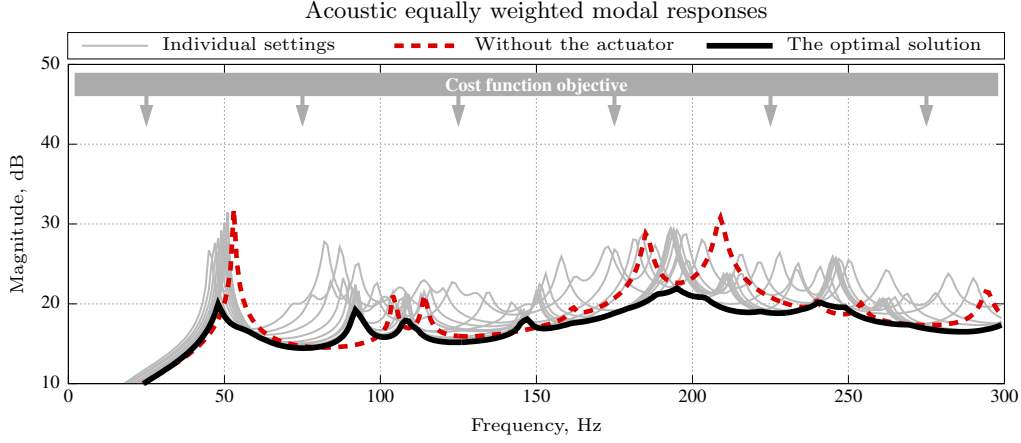
14

Figure 6: Acoustic equally weighted modal response of the panel, obtained for optimization index $J_1$ (solid gray lines — panel with the actuator set for different $z_{a,1}$, in the range from 0.01 m to 0.10 m, incremented by 0.01 m; dashed red line — the unloaded panel; solid black line — panel with optimally controlled semi-active mass). The actuator was attached at $x_{a,1} = 0.287$ m, $y_{a,1} = 0.098$ m, with $m_{a,1} = 0.081$ kg.

the unloaded panel (without the semi-active mass) is shown as a red dashed line. Comparing the optimal solution with the response of the unloaded panel, it can be seen that all of the strongest modes can be mitigated by more than 10 dB, assuming a single tonal or narrowband excitation at a time. The acoustic response of the panel can effectively be flattened by modifying the location of the mass, and only residual peaks are left. In nearly the entire frequency range, the optimal response of the loaded panel is lower than the response of the unloaded panel. Thus the conclusion can be drawn that this semi-active control approach is fully capable of avoiding the excitation of resonant frequencies of the whole panel by using only a single semi-active actuator.

Slightly different optimization results can be obtained by using a modified cost function $J_2$

$$J_2 = \max_f \left[ \min_{z_{a,1}} A(f, z_{a,1}) \right] . \tag{24}$$

The cost function $J_2$ results in the minimization of the acoustic radiation of the most radiating modes. While the cost function $J_1$ seeks for a wider trade-off and may allow slight increase of the acoustic radiation in one band, in exchange for a bigger reduction in another band, the cost function $J_2$ always takes into account only the highest peak in the acoustic response. It leads to as flatten acoustic response as possible. The algorithm achieved a solution with the actuator placed at $x_{a,1} = 0.261$ m, $y_{a,1} = 0.121$ m, with $m_{a,1} = 0.080$ kg. Results of this optimization are shown in Fig. 7. It can been seen in Fig. 7 that the response is quite similar to the previous one, although flattened even more at the expense of slight enhancements of the amplitude at some specific frequencies. However, these enhancements are practically negligible, hence the cost function $J_2$ can potentially provide even better solutions depending on the adopted objective.

It is worth mentioning that during practical operations, the individual responses of the barrier for different distances $z_{a,1}$ can be stored in a look-up table and, if needed, periodically experimentally recaptured in order to update the lookup table used for choosing the optimal configuration of $z_{a,1}$.

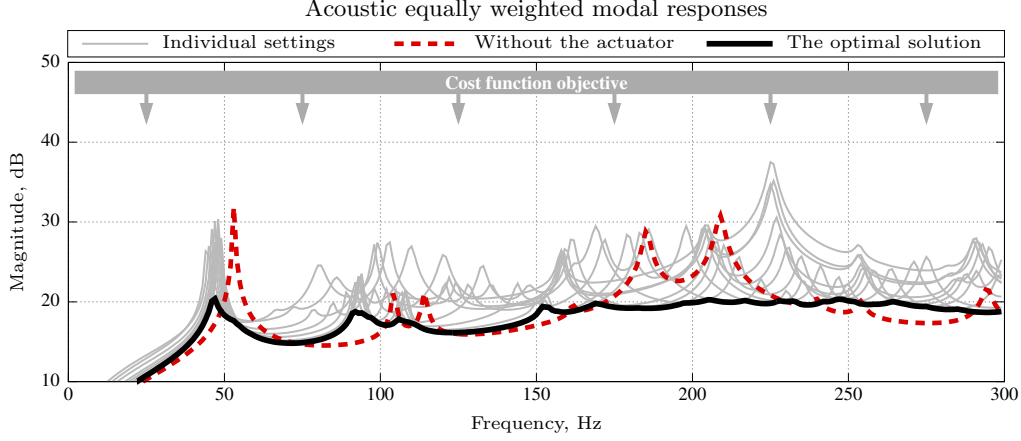Acoustic equally weighted modal responses



Figure 7: Acoustic equally weighted modal response of the panel, obtained for optimization index $J_2$ (solid gray lines — panel with the actuator set for different $z_{a,1}$, in the range from 0.01 m to 0.10 m, incremented by 0.01 m; dashed red line — the unloaded panel; solid black line — panel with optimally controlled semi-active mass). The actuator was attached at $x_{a,1} = 0.261$ m, $y_{a,1} = 0.121$ m, with $m_{a,1} = 0.080$ kg.

### 4.2. Semi-active sound source

In the second scenario, the panel is considered as an optimized structural sound source. The aim for the source is to radiate sound of a given frequency as efficiently as possible. To this end, the acoustic radiation of the panel should be maximized in the chosen frequency range. This objective is expressed using the following cost function

$$J_3 = \sum_{f=1}^{f=f_{max}} \left[ \max_{z_{a,1}} A(f, z_{a,1}) \right] , \qquad (25)$$

which maximizes the overall acoustic radiation of the panel.

The algorithm achieved a solution with the actuator placed at $x_{a,1} = 0.295$ m, $y_{a,1} = 0.213$ m, with $m_{a,1} = 0.161$ kg. Results of this optimization are shown in Fig. 8. In the considered scenario, the modal density of the panel is rather low, hence it is easier to shift resonances to avoid their excitation than it is to put them at any requested frequency. It would likely be easier to achieve a desired frequency if a higher mass were allowed, more actuators were used, or a panel of different parameters was introduced. Nevertheless, using the proposed semi-active approach, the acoustic response of the panel has been enhanced by approximately 10 dB for the majority of frequencies. Some gaps are visible where it was not possible to shift a resonance into a specific frequency interval. However, the response was definitely enhanced across the frequency range.

Following a modification analogous to the one used for $J_2$, a fourth cost function $J_4$ can be defined as

$$J_4 = \min f \left[ \max_{z_{a,1}} A(f, z_{a,1}) \right] , \qquad (26)$$

which focuses on eliminating gaps in the frequency response. In other words, the cost function $J_4$ takes into account only the lowest dip in the acoustic response. To enable the proper operation of $J_4$, the frequency range of interest was limited with a lower bound of 50 Hz, as lower frequencies are difficult to excite even with the action of the semi-active mass (the fundamental frequency
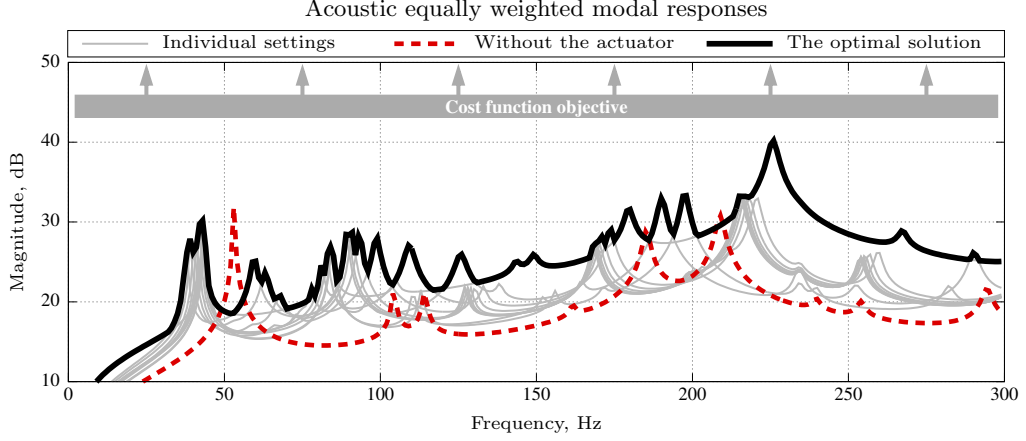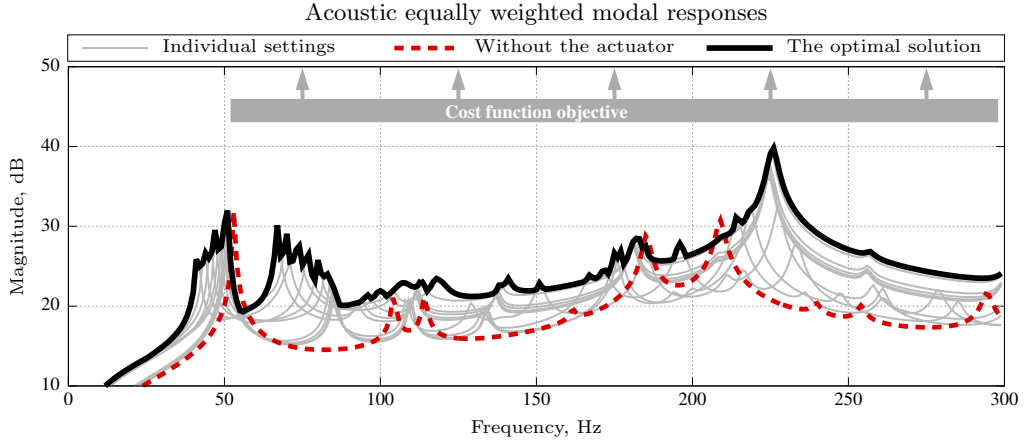
16

Acoustic equally weighted modal responses



Figure 8: Acoustic equally weighted modal response of the panel, obtained for optimization index $J_3$ (solid gray lines — panel with the actuator set for different $z_{a,1}$, in the range from 0.01 m to 0.10 m, incremented by 0.01 m; dashed red line — the unloaded panel; solid black line — panel with optimally controlled semi-active mass). The actuator was attached at $x_{a,1} = 0.295$ m, $y_{a,1} = 0.213$ m, with $m_{a,1} = 0.161$ kg.

Acoustic equally weighted modal responses



Figure 9: Acoustic equally weighted modal response of the panel, obtained for optimization index $J_4$ (solid gray lines — panel with the actuator set for different $z_{a,1}$, in the range from 0.01 m to 0.10 m, incremented by 0.01 m; dashed red line — the unloaded panel; solid black line — panel with optimally controlled semi-active mass). The actuator was attached at $x_{a,1} = 0.329$ m, $y_{a,1} = 0.291$ m, with $m_{a,1} = 0.147$ kg.

of the unloaded panel is approximately 50 Hz). The algorithm achieved a solution with the actuator placed at $x_{a,1} = 0.329$ m, $y_{a,1} = 0.291$ m, with $m_{a,1} = 0.147$ kg. The results of this optimization are shown in Fig. 9. It follows from analyzing this figure that $J_4$ is rather ineffective for the considered scenario due to the low modal density of the panel and the inevitable gaps in the response. However, the cost function $J_4$ is still worth mentioning as it is potentially more suitable for other panels with higher modal densities.

17

## 5. Semi-active control experiment

In this section additional verification experiments are performed for the optimal configuration followed from cost function $J_1$. The laboratory setup presented in Section 3 is used. The cost function $J_1$, as shown in Section 4, resulted in $x_{a,1} = 0.287$ m, $y_{a,1} = 0.098$ m, and $m_{a,1} = 0.081$ kg. Due to relatively low total mass, the moving mass was comparable with the mass of the actuator body. Hence, the range of $z_{a,1}$ was limited to a range between 0.03 m and 0.10 m.

Firstly, experimentally measured individual acoustic responses of the panel with the actuator set for different $z_{a,1}$ are given in Fig. 10. The figure corresponds to simulation results given in Fig. 5. Although there are discrepancies, partially due to uneven acoustic excitation, the predicted influence of the semi-active actuator actions is coherent with experimental results. Individual acoustic responses of the panel without the actuator and with the actuator set for $z_{a,1} = 0.05$ m are also compared with theoretical predictions in Fig. 11.

It is noteworthy that the impact of changing $z_{a,1}$ decreases for increasing frequencies. It is probably due to imperfect magnetic mounting (not perfectly rigid). A more rigid design should mitigate this issue. Nevertheless, in the frequency range up to 300 Hz a single semi-active actuator was able to achieve considerable reduction, often exceeding 10 dB (cf. Fig. 12). Results presented in Fig. 12 corresponds to simulation results given in Fig. 6. The predicted results of the semi-active control are coherent with the experiments. The authors believe that these results clearly presents the potential of the proposed semi-active control approach.

## 6. Conclusions

This paper proposes a novel semi-active actuator with tunable mass moment of inertia, capable of tuning the response of a panel during its operation. The actuator enables the adaptation of
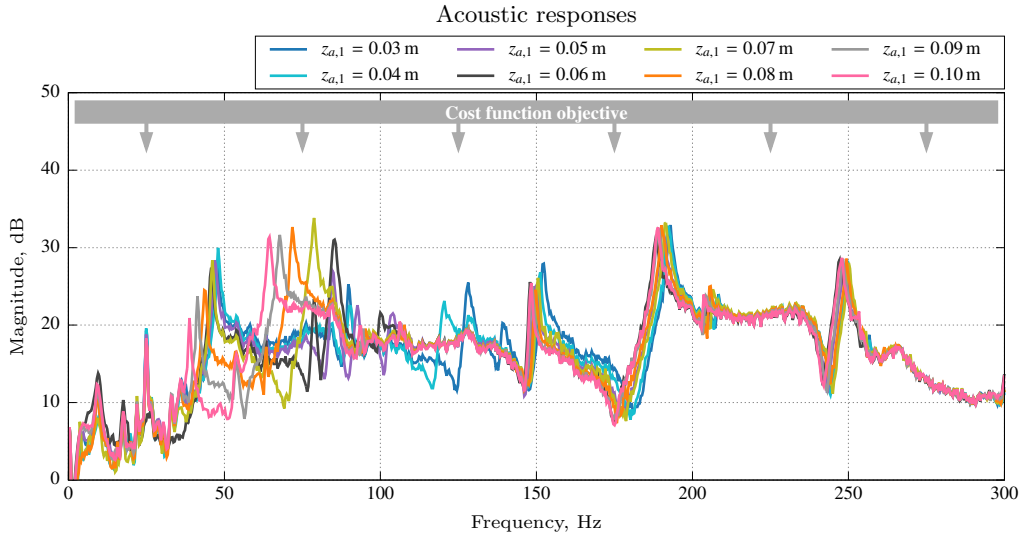


Figure 10: Experimentally measured individual acoustic responses of the panel, obtained for optimization index $J_1$, with the actuator set for different $z_{a,1}$, in the range from 0.03 m to 0.10 m, incremented by 0.01 m. The actuator was attached at $x_{a,1} = 0.287$ m, $y_{a,1} = 0.098$ m, with $m_{a,1} = 0.081$ kg. The figure corresponds to simulation results given in Fig. 5.

frequency-dependent transmission loss of a barrier to the current noise spectrum, and it can also be used to optimize acoustic radiation from a panel acting as a sound source.

A mathematical model of the panel with the proposed semi-active actuator has been derived and experimentally validated. An exemplary practical design of the proposed actuator has been presented. Subsequently, numerical simulation studies based on the validated model have been performed, providing analysis and insight into various practical aspects, including optimization of the location of the actuator according to proposed cost functions and the resulting acoustic performance. The concept of equally weighted modal response has been introduced into the
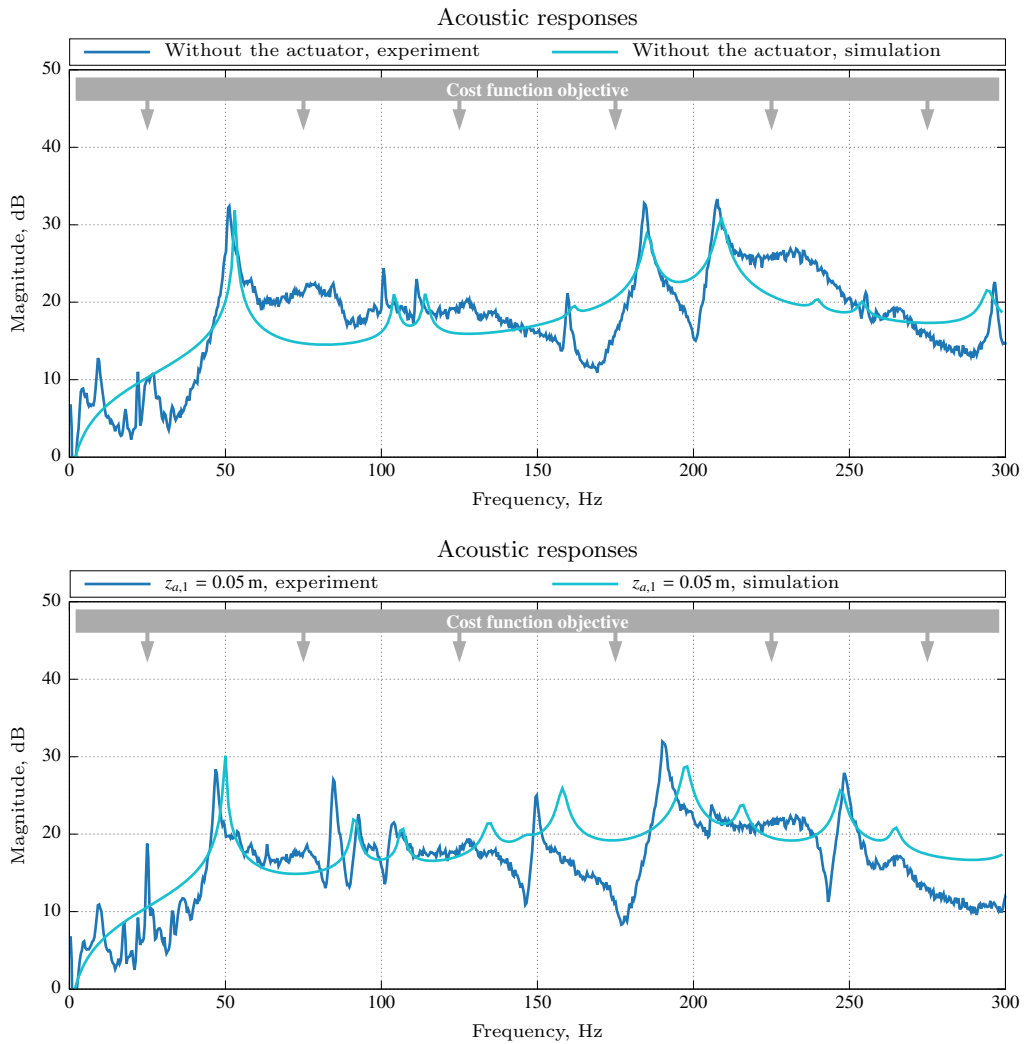


Figure 11: Experimentally measured and simulated individual acoustic responses of the panel, obtained for optimization index $J_1$, without the actuator (top) and with the actuator set for $z_{a,1} = 0.05$ m (bottom). The actuator was attached at $x_{a,1} = 0.287$ m, $y_{a,1} = 0.098$ m, with $m_{a,1} = 0.081$ kg.
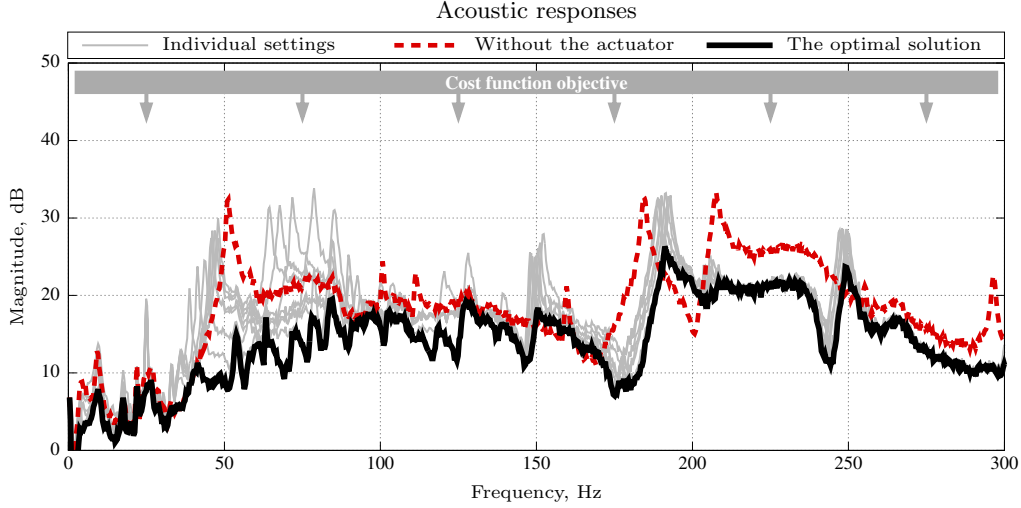
Figure 12: Experimentally measured acoustic response of the panel, obtained for optimization index $J_1$ (solid gray lines — panel with the actuator set for different $z_{a,1}$, in the range from 0.03 m to 0.10 m, incremented by 0.01 m; dashed red line — the unloaded panel; solid black line — panel with optimally controlled semi-active mass). The actuator was attached at $x_{a,1}$ = 0.287 m, $y_{a,1}$ = 0.098 m, with $m_{a,1}$ = 0.081 kg. The figure corresponds to simulation results given in Fig. 6.

optimization process in order to provide more general and practically-useful solutions.

As the presented results show, the proposed actuator can enhance the transmission loss of a noise barrier for time-varying tonal or narrow-band noise by more than 10 dB. In an alternative scenario where the panel is used as a sound source, by using the proposed semi-active approach the acoustic response of the panel can be enhanced by approximately 10 dB for the majority of frequencies.

This study shows that employment of even a single actuator provides substantial benefits. However, the utilization of multiple actuators would introduce more degrees of freedom and dimensions into the space of possible configurations of semi-active actuators, thus further extending the capabilities of the proposed approach. In addition, the proposed approach can be used to support active noise barriers [27], e.g. to enhance the controllability of inertial actuators for targeted frequency bands, thus forming a hybrid active/semi-active control system. Such an approach will be investigated by the authors in future research.

## Acknowledgment

## References

[1] K. Ege, M. Gallo, Q. Leclere, R. Rinaldi, N. B. Roozen, N. Totaro, Modeling, designing and measuring hybrid sandwich composite panels with optimized damping properties, in: Acoustic Black Holes and Structured Plates for Vibration Control, ABH2018, Le Mans, France, 2018.

[2] Y. Li, L. Cheng, Mechanisms of active control of sound transmission through a linked double-wall system into an acoustic cavity, Applied Acoustics 69 (7) (2008) 614–623. `doi:10.1016/j.apacoust.2007.02.001`.

[3] S. Wrona, M. Pawelczyk, Active reduction of device narrowband noise by controlling vibration of its casing based on structural sensors, in: Proceedings of 22nd International Congress on Sound and Vibration, Florence, Italy, 12-16 July, 2015.

[4] H. Ji, X. Wang, J. Qiu, L. Cheng, Y. Wu, C. Zhang, Noise reduction inside a cavity coupled to a flexible plate with embedded 2-d acoustic black holes, Journal of Sound and Vibration 455 (2019) 324–338. `doi:10.1016/j.jsv.2019.05.004`.

[5] M. Misol, S. Algermissen, M. Rose, H. P. Monner, Aircraft lining panels with low-cost hardware for active noise reduction, in: 2018 Joint Conference-Acoustics, IEEE, 2018, pp. 1–6. `doi:10.1109/ACOUSTICS.2018.8502310`.

[6] N. Kournoutos, J. Cheer, Directivity control using a structural actuator array, in: Proceedings of 26th International Congress on Sound and Vibration, Montreal, Canada, 7-11 July, 2019.

[7] K.-H. Lee, J.-G. Ih, A simulation study on the array control of a rectangular panel speaker for improving the sound radiation performance, Journal of Sound and Vibration 488 (2020) 115631. `doi:10.1016/j.jsv.2020.115631`.

[8] S. Wrona, M. Pawelczyk, Shaping frequency response of a vibrating plate for passive and active control applications by simultaneous optimization of arrangement of additional masses and ribs. Part I: Modeling, Mechanical Systems and Signal Processing 70-71 (2016) 682–698. `doi:10.1016/j.ymssp.2015.08.018`.

[9] S. Wrona, K. Mazur, J. Rzepecki, A. Chraponska, M. Pawelczyk, Sound transmission through a thin plate with shaped frequency response, Archives of Acoustics 44 (4) (2019) 731–738. `doi:10.24425/aoa.2019.129728`.

[10] S. Wrona, M. Pawelczyk, X. Qiu, Shaping the acoustic radiation of a vibrating plate, Journal of Sound and Vibration (2020) 115285`doi:10.1016/j.jsv.2020.115285`.

[11] G. S. Sharma, A. Sarkar, Directivity-based passive barrier for local control of low-frequency noise, Journal of Theoretical and Computational Acoustics 26 (04) (2018) 1850012. `doi:10.1142/S2591728518500123`.

[12] G. S. Sharma, A. Sarkar, Directivity based control of acoustic radiation, Applied Acoustics 154 (2019) 226–235. `doi:10.1016/j.apacoust.2019.04.031`.

[13] P. R. Budarapu, T. Narayana, B. Rammohan, T. Rabczuk, Directionality of sound radiation from rectangular panels, Applied Acoustics 89 (2015) 128–140.

[14] L.-L. Chung, Y.-A. Lai, C.-S. W. Yang, K.-H. Lien, L.-Y. Wu, Semi-active tuned mass dampers with phase control, Journal of Sound and Vibration 332 (15) (2013) 3610–3625. `doi:10.1016/j.jsv.2013.02.008`.

[15] M. D. Christie, S. Sun, L. Deng, D. Ning, H. Du, S. Zhang, W. Li, The variable resonance magnetorheological pendulum tuned mass damper: Mathematical modelling and seismic experimental studies, Journal of Intelligent Material Systems and Structures 31 (2) (2020) 263–276.

[16] T. Ehrig, M. Dannemann, R. Luft, C. Adams, N. Modler, P. Kostka, Sound transmission loss of a sandwich plate with adjustable core layer thickness, Materials 13 (18) (2020) 4160. `doi:10.3390/ma13184160`.

[17] S. S. Rao, Vibration of continuous systems, Vol. 464, Wiley Online Library, 2007.

[18] D. Young, Vibration of rectangular plates by the ritz method, Journal of Applied Mechanics-Transactions of the ASME 17 (4) (1950) 448–453.

[19] S. Wrona, M. Pawelczyk, Shaping frequency response of a vibrating plate for passive and active control applications by simultaneous optimization of arrangement of additional masses and ribs. Part II: Optimization, Mechanical Systems and Signal Processing 70-71 (2016) 699–713. `doi:10.1016/j.ymssp.2015.08.017`.

[20] K. Kim, B.-H. Kim, T.-M. Choi, D.-S. Cho, Free vibration analysis of rectangular plate with arbitrary edge constraints using characteristic orthogonal polynomials in assumed mode method, International Journal of Naval Architecture and Ocean Engineering 4 (3) (2012) 267–280. `doi:10.2478/ijnaoe-2013-0095`.

[21] R. R. Craig, A. J. Kurdila, Fundamentals of structural dynamics, John Wiley & Sons, 2006.

[22] A. N. Norris, D. M. Photiadis, Thermoelastic relaxation in elastic structures, with applications to thin plates, The Quarterly Journal of Mechanics and Applied Mathematics 58 (1) (2005) 143–163. `doi:10.1093/qjmamj/hbi002`.

[23] S. Leleu, H. Abou-Kandil, Y. Bonnassieux, Piezoelectric actuators and sensors location for active control of flexible structures, in: Proceedings of the 17th IEEE Instrumentation and Measurement Technology Conference, Vol. 2, IEEE, 2000, pp. 818–823. `doi:10.1109/IMTC.2000.848848`.

[24] W. Rdzanek, Structural vibroacoustics of surface elements [in Polish: Wibroakustyka strukturalna elementów powierzchniowych], Rzeszów University of Technology Publishing House, 2011.

[25] S. Wrona, M. Pawelczyk, Identification of elastic boundary conditions of light-weight device casing walls using experimental data, in: Proceedings of 21st International Conference On Methods and Models in Automation and Robotics (MMAR), IEEE, Midzyzdroje, Poland, 29 August - 1 September, 2016. `doi:10.1109/MMAR.2016.7575135`.

[26] F. Neri, C. Cotta, P. Moscato, Handbook of memetic algorithms, Vol. 379, Springer, 2012.

[27] K. Mazur, S. Wrona, M. Pawelczyk, Active noise control for a washing machine, Applied Acoustics 146 (2019) 89–95. `doi:10.1016/j.apacoust.2018.11.010`.